24th INTERNATIONAL CONGRESS ON SOUND AND VIBRATION
23–27 July 2017, London

ICSV24
23-27JULY 2017
LONDON CALLING

VIBRATION OF AN EXPONENTIALLY TAPERED ROD EMBEDDED IN AN ELASTIC SOLID - A PIECEWISE UNIFORM APPROACH

Michał K. Kalkowski, Jen M. Muggleton and Emiliano Rustghi
Institute of Sound and Vibration Research, University of Southampton, Highfield, Southampton SO17 1BJ, UK
email: M.Kalkowski@soton.ac.uk

Exponentially tapered rods can serve as a simplified physical model for tree roots. Based on an analytical solution for axial waves in a uniform embedded rod, we present a piecewise uniform formulation for modelling the dynamics of a tapered embedded rod. First, we revisit the uniform rod solution and discuss its characteristics. The piecewise uniform approach, in which the tapered rod is approximated as a multi-step structure composed of a number of uniform components, is presented next. The dynamics of the built-up waveguide are written in terms of propagating waves that scatter at the junctions. The assumption is made that the surrounding elastic medium has no effect on the scattering. We conduct a numerical convergence study and verify the accuracy of our model against an axisymmetric finite element (FE) simulation with perfectly absorbing boundaries. Both predictions are in very good agreement except for the low frequency range, where an assumption regarding the boundary contidions is expected to play a role. Finally, some basic observations are given in the context of the dynamics of a free tapered rod.

Keywords: embedded rod, axial waves, roots

Introduction

The interest in vibration of embedded structures has typically been motivated by applications related to infrastructure, such as building foundations, tunnels, or buried pipework. For the former two examples, the focal points include reduction of vibration transmission from the ground to the building, or from the tunnel to the ground. For the latter wave radiation is actually found useful for determining the location of buried pipes and assessing its state. A large number of solutions have been developed for a vast range of engineering scenarios. However, to our best knowledge, waves in embedded tapered rods have not been addressed yet.

At first, such structure may seem to be of little practical relevance. However, based on the descriptions given by tree physiologists [1], an embedded, exponentially tapered rod can serve as a good physical model for a tree root in soil. An insight into the waves in root-like structures is expected to inform non-destructive root detection from surface vibration measurements. Such technique has proven to be effective for locating buried water pipes [2].

Some fundamental dynamics of exponentially tapered structures was addressed in our previous work [3] where we established a method for estimating wavenumbers in tapered rods from five equispaced vibration responses. In this paper, we focus on the effect of the surrounding medium on propagating waves. Our interest is confined to descriptions originating from analytical formulations.

There is a relatively small number of publications addressing specifically axial waves in embedded rods and all of them treat uniform rods only. Toki and Takada [4] formulated equations for both

axial and bending strains in underground tubular structures aiming to inform earthquake-resistant design of buried infrastructure. Their predictions were further refined and extended by Parnes and his collaborators [5, 6, 7]. Ground surface response to waves propagating along a buried pipe was analysed by Jette and Parker [8], and more recently by [9, 10, 11] where the internal fluid and various coupling conditions between the pipe and the soil were analysed. An experimental investigation into waves in a pipe buried in sand was also published recently [12].

To our best knowledge, no description of the dynamics of embedded tapered structures is available. In this paper we address this topic, starting from the uniform rod formulation and constructing a piecewise uniform model to represent the tapered geometry. Predictions of this semi-analytical approach are validated with axisymmetric finite elements, and several physical aspects are discussed.

Axial waves in a uniform rod embedded in an elastic medium

In this section, the dispersion relation for axial waves in a uniform rod embedded in an solid medium is derived based on the elementary rod theory and the Navier's displacement equation, respectively. The coupling between the rod and an infinite medium is represented by surface traction restraining the rod and. The general form of the governing equation for a uniform, embedded rod is adopted from Parnes [6], but in this paper it is solved using different soil dynamics formulations

Governing equation

We consider a circular rod and denote z as the propagation direction and r as the radial direction. The equation of motion for the rod is written as

$$EA\frac{\partial^2 u_{\text{rod}}}{\partial z^2} + \int_S \tau_{rz}(a)\,\mathrm{d}S - \rho A\frac{\partial^2 u_{\text{rod}}}{\partial t^2} = 0 \tag{1}$$

where E is the Young's modulus, A is the cross-sectional area, ρ is the density, τ_{rz} is the transverse shear traction, S is the circumference and u_{rod} is the displacement of the rod. The integral of traction is simply: $\int_S \tau_{rz}(a)\,\mathrm{d}S = 2\pi a\tau_{rz}(a)$ where a is the radius of the rod. Rearranging the governing equation, one obtains

$$E\frac{\partial^2 u_{\text{rod}}}{\partial z^2} + \frac{2\pi a}{A}\tau_{rz}(a) - \rho\frac{\partial^2 u_{\text{rod}}}{\partial t^2} = 0 \tag{2}$$

which after assuming the motion to be spatially and temporally harmonic, can be written as

$$-Ek^2 U_{\text{rod}} + \frac{2\pi a}{A}\tau_{rz}(a) + \rho\omega^2 U_{\text{rod}} = 0 \tag{3}$$

To enable the traction to be expressed in terms of U_{rod}, one needs to consider wave propagation in the surrounding medium and the displacement continuity condition.

Waves in soil

In the following paragraphs, the equations for cylindrical wave propagation in an infinite elastic medium are presented, largely after Kolsky [13]. The displacement vector is defined as

$$\mathbf{u} = \begin{bmatrix} u_r & u_\theta & u_z \end{bmatrix} \tag{4}$$

The strains can be written as

$$\begin{aligned} \epsilon_{rr} &= \frac{\partial u_r}{\partial r} & \epsilon_{\theta\theta} &= \frac{1}{r}\frac{\partial u_\theta}{\partial \theta} + \frac{u_r}{r} & \epsilon_{zz} &= \frac{\partial u_z}{\partial z} \\ \epsilon_{r\theta} &= \frac{1}{2}\left(\frac{1}{r}\frac{\partial u_r}{\partial \theta} + \frac{\partial u_\theta}{\partial \theta} - \frac{u_\theta}{r}\right) & \epsilon_{rz} &= \frac{1}{2}\left(\frac{\partial u_z}{\partial r} + \frac{\partial u_r}{\partial z}\right) & \epsilon_{\theta z} &= \frac{1}{2}\left(\frac{\partial u_\theta}{\partial z} + \frac{1}{r}\frac{\partial u_z}{\partial \theta}\right) \end{aligned} \tag{5}$$

The curl of the displacement vector $\mathbf{u}$ is expressed in terms of rotations around the orthogonal axes

$$\frac{1}{2}\operatorname{curl}\mathbf{u} = \frac{1}{2}\nabla\times\mathbf{u} = \begin{bmatrix}\varpi_r & \varpi_\theta & \varpi_z\end{bmatrix} \tag{6}$$

where

$$\begin{aligned}\varpi_r &= \frac{1}{2}\left(\frac{1}{r}\frac{\partial u_z}{\partial\theta} - \frac{\partial u_\theta}{\partial z}\right)\\ \varpi_\theta &= \frac{1}{2}\left(\frac{\partial u_r}{\partial z} - \frac{\partial u_z}{\partial r}\right)\\ \varpi_z &= \frac{1}{2r}\left[\frac{\partial(ru_\theta)}{\partial r} - \frac{\partial u_r}{\partial\theta}\right]\end{aligned} \tag{7}$$

The motion of the soil is governed by the Navier's displacement equation

$$(\lambda+\mu)\nabla\Delta + \mu\nabla^2\mathbf{u} = \rho\frac{\partial^2\mathbf{u}}{\partial t^2} \tag{8}$$

where the dilatation Δ in cylindrical coordinates is

$$\Delta = \frac{1}{r}\frac{\partial(ru_r)}{\partial r} + \frac{1}{r}\frac{\partial u_\theta}{\partial\theta} + \frac{\partial u_z}{\partial z} \tag{9}$$

Both the tangential displacement u_θ and variation of the other components along the θ direction vanish under the axisymmetric motion assumption. The dillatation and rotation equations are then simplified, leading to

$$\begin{aligned}\frac{\partial^2\Delta}{\partial r^2} + \frac{1}{r}\frac{\partial\Delta}{\partial r} + (k_L^r)^2\Delta = 0\\ \frac{\partial^2\varpi_\theta}{\partial r^2} + \frac{1}{r}\frac{\partial\varpi_\theta}{\partial r} - \frac{\varpi_\theta}{r^2} + (k_S^r)^2\varpi_\theta = 0\end{aligned} \tag{10}$$

where k_S^r and k_L^r are the projections of the bulk wavenumbers onto the radial direction. The above are Bessel equations, and their solutions for outgoing waves can be written using Hankel functions (which are combinations of linearly independent Bessel functions)

$$\begin{aligned}\Delta &= BH_0^{(2)}(k_L^r r)\\ \varpi_\theta &= DH_1^{(2)}(k_S^r r)\end{aligned} \tag{11}$$

Throughout the following derivations, Hankel functions of the second kind are used since the time-harmonic motion is represented using $\mathrm{e}^{\jmath\omega t}$ component. For convenience, the subscript denoting the kind is dropped hereafter. The soil displacements are assumed to be of the form

$$\begin{aligned}u_r &= U\mathrm{e}^{\jmath(\omega t - kz)}\\ u_z &= W\mathrm{e}^{\jmath(\omega t - kz)}\end{aligned} \tag{12}$$

Substituting them into the expression for dilatation and rotation we obtain

$$\begin{aligned}\Delta &= \left[\frac{\partial U}{\partial r} + \frac{U}{r} - \jmath kW\right]\\ 2\varpi_\theta &= \left[-\jmath kU - \frac{\partial W}{\partial r}\right]\end{aligned} \tag{13}$$

where the space-time harmonic term was ommitted for brevity. Kolsky [13] proposes the following form of U and W to satisfy the above equations

$$\begin{aligned}U &= C_1\frac{\partial}{\partial r}H_0(k_L^r r) - C_2 kH_1(k_S^r r) = -C_1(k_L^r)H_1(k_L^r r) - C_2 kH_1(k_S^r r)\\ W &= -\jmath kC_1H_0(k_L^r r) + \frac{\jmath C_2}{r}\frac{\partial}{\partial r}[rH_1(k_S^r r)] = -\jmath kC_1H_0(k_L^r r) + \jmath C_2 k_s^r H_0(k_S^r r)\end{aligned} \tag{14}$$

Table 1: Material properties used in predictions.

material	E, GPa	μ, MPa	ν	ρ, kg m^{-3}
root	14	-	-	540
soil	-	15	0.33	1500

The relationship between the constants C_1 and C_2 is established by assuming that the rod is rigid in the r direction. Finally, after some arithmetic manipulations, an expression for the shear stress on the surface of the rod is obtained

$$\tau_{rz}|_{r=a} = \mu \frac{\partial W}{\partial r}|_{r=a} = \mu \left[\jmath k k_L^r C_1 H_1(k_L^r a)\right] \frac{(k_S)^2}{k^2} \tag{15}$$

Rod-soil interface

The displacement continuity condition states that

$$u_{\text{rod}}(z,t) = u_z(a,z,t) \tag{16}$$

which results in

$$C_1 = -\frac{U_{\text{rod}}}{\jmath k H_1(k_L^r a)} \left\{ \left[\frac{H_0(k_L^r a)}{H_1(k_L^r a)} + \frac{k_L^r k_S^r}{k^2} \frac{H_0(k_S^r a)}{H_1(k_S^r a)} \right] \right\}^{-1} \tag{17}$$

Coupled dispersion equation

Equations (15) and (17) can now be substituted into Eq. (3)

$$-k^2 E - \frac{2\mu k_L^r}{a} \left[F(k_L^r a) + \frac{k_L^r k_S^r}{k^2} F(k_S^r a) \right]^{-1} \frac{(k_S)^2}{k^2} + \rho\omega^2 = 0 \tag{18}$$

where

$$F(s) = \frac{H_0(s)}{H_1(s)} \tag{19}$$

After several rearrangements and simplifications we obtain

$$k^4 + k^2 \left[k_L^r k_S^r \frac{F(k_S^r a)}{F(k_L^r a)} - \frac{\omega^2}{c_0^2} \right] - \frac{\omega^2}{c_0^2} k_L^r k_S^r \frac{F(k_S^r a)}{F(k_L^r a)} + \frac{2\mu k_L^r}{EaF(k_L^r a)} (k_S)^2 = 0 \tag{20}$$

where c_0 is the free rod wavespeed. The above is a biquadratic equation in k. If one assumes that the wavelength in the rod is much longer than in the surrounding soil, the projections of bulk wavenumbers onto the radial direction may be approximated as the bulk wavenumbers themselves ($k_{L,S}^r \approx k_{L,S}$). This enables the wavenumbers to be identified from Eq. (20) directly.

The solution of Eq. (20) yields two wavenumbers, only one of which corresponds to a physical solution (the other implies the growth of the wave and unbounded wavespeed). In Fig. 1 we plotted the phase velocity and attenuation for that wave together with a reference result obtained using a semi-analytical finite element method and bulk wave velocities. The radius was taken as $a = 0.1$ m and respective material properties are gathered in Table 1. It is confirmed that Eq. (20) gives an accurate prediction of the axial wavenumber (below the cut-off frequency of the first higher-order wave). One may also notice that at higher frequencies, the phase velocity tends to that of a free rod.

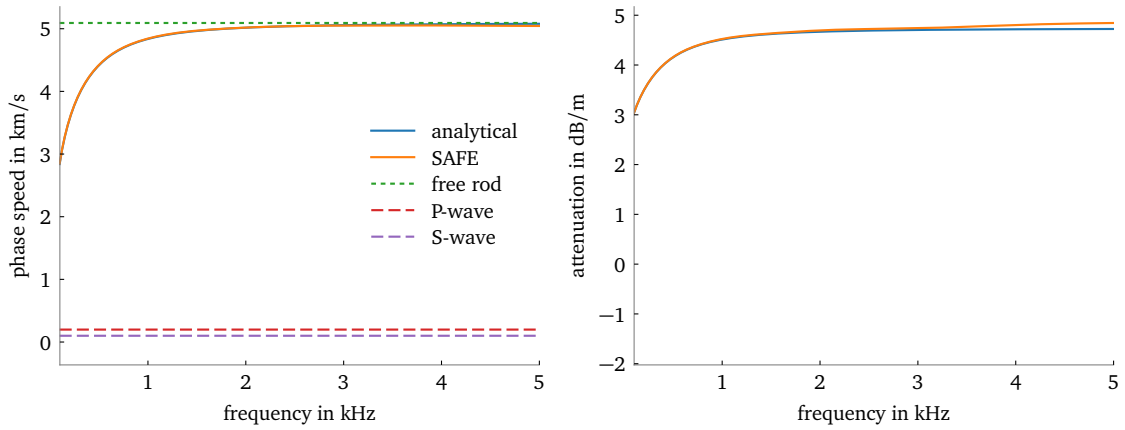

Figure 1: Phase velocity and attenuation for a uniform embedded rod – comparison between the analytical model and a numerical prediction based on a SAFE-PML approach.

Piecewise uniform model for a tapered embedded rod

In this section a piecewise uniform model for an exponentially tapered embedded rod is considered. The variation of the radius is assumed to be

$$r(z) = a\mathrm{e}^{-\beta z} \tag{21}$$

where a is the starting radius and β is the flare constant. In such case, no analytical solution is available, as the coefficients in Eq. (1) are not constant any more. Furthermore, we note that the wavenumber depends on the radius of the cross-section and therefore would vary with position for a tapered rod.

As an alternative, the tapering is represented as a series of discrete steps. The buried tapered rod is thought to be composed of a large number of uniform segments, each of which can be described by equations derived in the previous section, resulting in a piecewise uniform model. It is assembled using an approach outlined in our previous work (see the appendix in [3] and a related supplementary material [14] for code). For brevity, the assembly process is not presented here, and the reader is referred to these references for further details.

In the following it is discussed how the neighbouring elements are coupled or, in other words, how the scattering matrices are calculated. First, for the piecewise uniform model, the non-physical solution to Eq. (20) is disregarded. There is only one degree of freedom allowed in the rod model. At each junction, the usual displacement continuity and force equilibrium must hold and these are the preliminaries for scattering matrix calculation. The resultant force over the cross section is calculated as

$$P = EA\frac{\partial u}{\partial z} = -\jmath kEAq^+ + \jmath kEAq^- = Dq^+ - Dq^- \tag{22}$$

where D is defined in the last step.

Consider a junction between two rod elements with different radii, denoted by a and b. We can write the displacement continuity and force equilibrium equations in a matrix form

$$\begin{bmatrix} 1 & 1 \\ D_a & -D_a \end{bmatrix} \begin{Bmatrix} q_a^+ \\ q_a^- \end{Bmatrix} = \begin{bmatrix} 1 & 1 \\ D_b & -D_b \end{bmatrix} \begin{Bmatrix} q_b^+ \\ q_b^- \end{Bmatrix} \tag{23}$$

Note that waves q_a^+ and q_b^- are incident upon the junction, whereas waves q_a^- and q_b^+ are leaving the junction. In this formulation, any additional radiation effects related to the discontinuity are neglected, i.e. scattering matrices are calculated in the same way as for an unrestrained rod. Equation

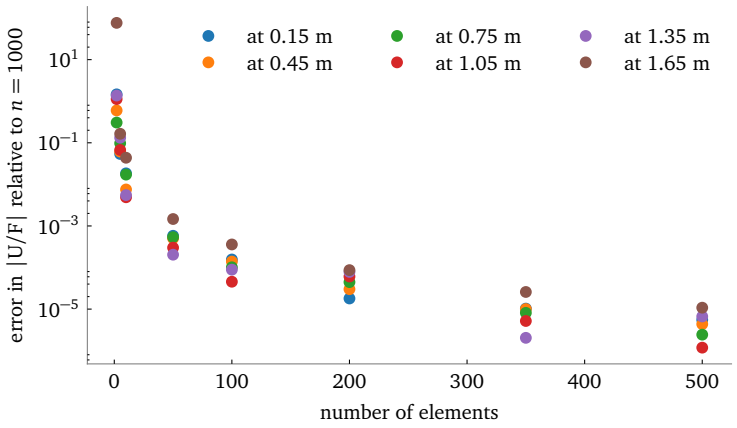

Figure 2: Relative error of the magnitude of the receptance averaged across the frequency range between 1 Hz and 3 kHz as a function of the number of elements.

(23) can now be rearranged to express waves leaving the junctions in terms of waves incident upon the junction, enabling the scattering matrix to be calculated as

$$\begin{Bmatrix} q_a^- \\ q_b^+ \end{Bmatrix} = \frac{1}{D_a + D_b} \begin{bmatrix} D_a - D_b & 2D_b \\ 2D_a & D_b - D_a \end{bmatrix} \begin{Bmatrix} q_a^+ \\ q_b^- \end{Bmatrix} \tag{24}$$

The excitation is applied at the large face of the rod resulting in an excited wave of amplitude

$$e^+ = \frac{1}{-D_0} \tag{25}$$

where the subscript 0 denotes that the expression refers to the first piecewise element. In this model, we assume that the reflection coefficients at both ends of the rod are the same as for a free end ($R_R = R_L = 1$). The fine tip could be treated as stiffness constrained, where the stiffness is a frequency dependent term appropriately deduced from the governing equation.

Convergence

To establish how the rate at which the piecewise uniform model converges, a series of calculations for the same structure with increasing number of elements were conducted. Material properties are the same as in Table 1 with the exception that we added a loss factor for soil ($\eta = 0.1$). The starting radius was taken as $a = 0.1$ m, the flare constant as $\beta = 1.6$ and the length as $L = 2$ m. The results of the study, presented in Fig. 2, suggest that a relatively small number of elements is required to achieve acceptable accuracy. In the considered example 50 elements suffice to achieve an relative error of $\approx 0.1\%$ with reference to the finest grid ($n = 1000$).

Numerical verification against finite element simulations

The predictions of the piecewise model were compared to a finite element simulation (COMSOL). Since the interest was confined to axial waves, the domain was assumed axisymmetric. The soil surrounding the root was modelled using a quarter of an ellipsoid, to resemble the configuration of the analytical model (see Fig. 3a). The excitation force was applied to the large face of the rod as a boundary load and dynamic responses were recorded at six points along its length (0.15, 0.45, 0.75, 1.05, 1.35 and 1.65 m from the force location). The infinite extent of the soil was represented by a low-reflecting boundary at the convex surface of the ellipsoid (parameters automatically adjusted by COMSOL).

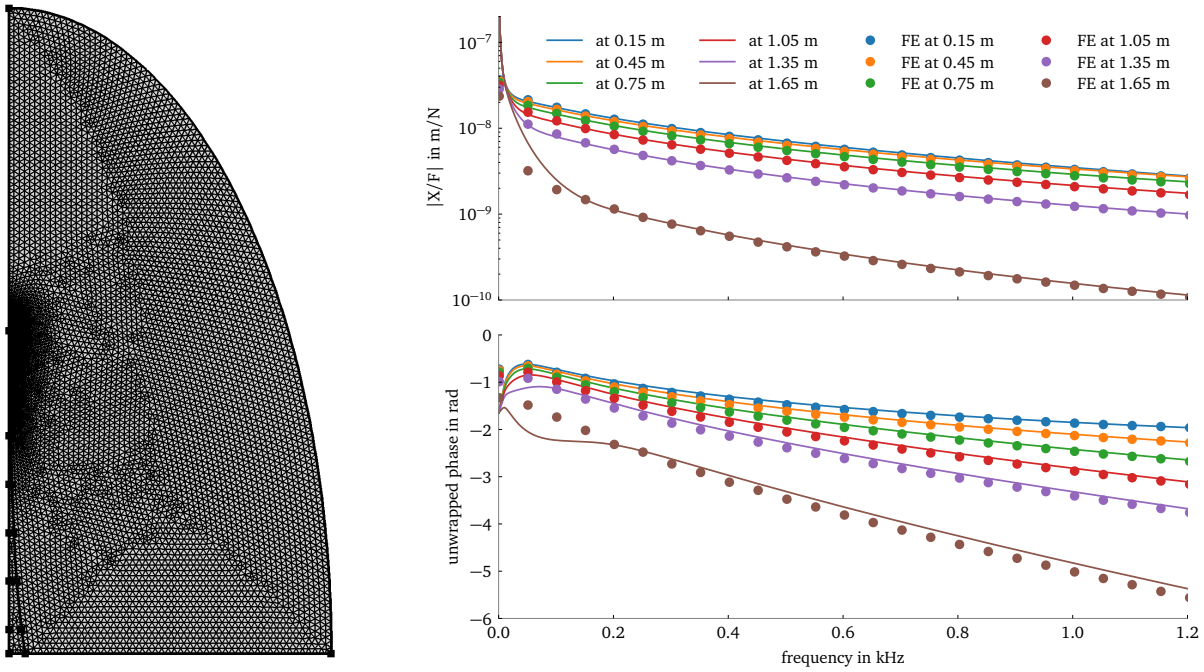

(a) (b)

Figure 3: Numerical validation against finite elements: (a) FE model (14145 elements); (b) frequency response functions predicted by the presented model ($n = 50$) and by the axisymmetric FE model.

The receptances plotted as magnitudes and frequency-unwrapped phases are shown in Fig. 3b. The results agree very well across most of the frequency range, confirming the validity of the piecewise uniform model. Discrepancies at low frequencies are attributed to the fact that the tip end is assumed free in our model, hence the whole structure has a rigid body mode at zero frequency. This is not the case for the finite element model, where the response reflect the apparent infinite extend of the soil.

Discussion

Presented frequency response function offer some fundamental insights into wave motion in such a structure. We note that the unwrapped phases (in particular, their slopes) correspond to the wavenumbers, whereas the magnitudes reflect wave attenuation. Results from Fig. 3b indicate that, unlike in a free tapered rod, waves decay towards the fine tip, as they radiate into the surrounding medium. By accounting for the locations of the points where the responses were computed, one acknowledges that the attenuation grows towards the fine tip. The variation of the wavenumber is not immediately apparent from Fig. 3b. However, since the wavenumber in an embedded uniform rod depends on the radius, we expect that this is, indeed, the case. Finally, contrary to what is observed in free tapered rods, there is no cut-off region for axial waves as they propagate from zero frequency. Despite the computational issues reaching beyond the scope of the present article, we note that the piecewise uniform formulation is at least a couple of orders of magnitude faster than the commercial finite element solution.

Conclusions

In this paper we focused on predicting the dynamics of an exponentially tapered rod embedded in a solid medium. We first derived a dispersion equation for axial waves in a uniform embedded

rod and used it in a piecewise uniform formulation which allowed for representing the varying geometry. A convergence study indicated that a relatively small number of elements was required to get satisfactory predictions. Finally, the piecewise uniform model was verified with a finite element simulation, showing very good agreement. It was observed that, unlike in the free tapered rod, there is no cut-off region for an axial wave and that it decays towards the fine tip owing to radiation. Finally, the wavenumber for embedded rods depends on the radius, so for tapered rods in soil it is position-dependent. Future work will include a further exploration of the physics behind the observed phenomena, also for flexural waves, and an experimental validation.

Acknowledgements

Funding: The support provided by the EPSRC (under grant EP/K021699/1) is gratefully acknowledged.

REFERENCES

1. Wilson, B. F., *The Growing Tree*, Univ of Massachusetts Press (1984).
2. Muggleton, J. M., Brennan, M. J. and Gao, Y. Determining the location of buried plastic water pipes from measurements of ground surface vibration, *Journal of Applied Geophysics*, **75** (1), 54–61, (2011).
3. Kalkowski, M. K., Muggleton, J. M. and Rustighi, E. An experimental approach for the determination of axial and flexural wavenumbers in circular exponentially tapered bars, *Journal of Sound and Vibration*, **390**, 67–85, (2017).
4. Toki, K. and Takada, S. Earthquake response analysis of underground tubular structure, *Bulletin of the Disaster Prevention Research Institute*, **24** (2), 107–125, (1974).
5. Parnes, R. and Weidlinger, P. Dynamic interaction of an embedded cylindrical rod under axial harmonic forces, *International Journal of Solids and Structures*, **17** (9), 903–913, (1981).
6. Parnes, R. Dispersion relations of waves in a rod embedded in an elastic medium, *Journal of Sound and Vibration*, **76** (1), 65–75, (1981).
7. Parnes, R. Torsional dispersion relations of waves in an infinitely long clad cylindrical rod, *The Journal of the Acoustical Society of America*, **71** (6), 1347–1351, (1982).
8. Jette, A. N. and Parker, J. G. Surface displacements accompanying the propagation of acoustic waves within an underground pipe, *Journal of Sound and Vibration*, **69** (2), 265–274, (1980).
9. Muggleton, J. M., Brennan, M. J. and Pinnington, R. J. Wavenumber prediction of waves in buried pipes for water leak detection, *Journal of Sound and Vibration*, **249** (5), 939–954, (2002).
10. Muggleton, J. M. and Yan, J. Wavenumber prediction and measurement of axisymmetric waves in buried fluid-filled pipes: Inclusion of shear coupling at a lubricated pipe/soil interface, *Journal of Sound and Vibration*, **332** (5), 1216–1230, (2013).
11. Gao, Y., Sui, F., Muggleton, J. M. and Yang, J. Simplified dispersion relationships for fluid-dominated axisymmetric wave motion in buried fluid-filled pipes, *Journal of Sound and Vibration*, **375**, 386–402, (2016).
12. Leinov, E., Lowe, M. J. S. and Cawley, P. Investigation of guided wave propagation and attenuation in pipe buried in sand, *Journal of Sound and Vibration*, **347**, 96–114, (2015).
13. Kolsky, H., *Stress Waves in Solids*, Oxford University Press, London, UK (1953).
14. Kalkowski, M. K. Supplementary material to 'An experimental approach for the determination of axial and flexural wavenumbers in circular exponentially tapered bars' : First release, *Zenodo*, **DOI: 10.5281/zenodo.583136**, (2017).